*materials*

MDPI

*Article*

# Effect of $CO_2$ on the Desulfurization of Sintering Flue Gas with Hydrated Lime

**Jianguo Hong [1,2], Xinqing Zou [1], Ziqiang Qin [1], Bin Zhou [1], Shuhua Geng [1,*], Yuwen Zhang [1,*], Xingli Zou [1] and Xionggang Lu [1,*]**

[1] State Key Laboratory of Advanced Special Steel & Shanghai Key Laboratory of Advanced Ferrometallurgy & School of Materials Science and Engineering, Shanghai University, Shanghai 200444, China
[2] Ironmaking Plant, Shanghai Meishan Iron and Steel Co., Ltd., Nanjing 210039, China
* Correspondence: shgeng@i.shu.edu.cn (S.G.); springzyw@shu.edu.cn (Y.Z.); luxg@shu.edu.cn (X.L.)

**Abstract:** The effect of carbon dioxide ($CO_2$) on the desulfurization of sintering flue gas with hydrate ($Ca(OH)_2$) as an absorbent was investigated, and the formation of calcium carbonate ($CaCO_3$) and its effect on the desulfurization was discussed. The competitive relationship between carbon dioxide ($CO_2$) and sulfur dioxide ($SO_2$) with the deacidification agent in sintering flue gas is discussed thermodynamically, showing that sulfates are more likely to be generated under high oxygen potential conditions and that $SO_2$ reacts more preferentially than $CO_2$ under a thermodynamic standard state. The amount of produced $CaCO_3$ increases under the condition that the $CO_2$ concentration is absolutely dominant to $SO_2$ in the sintering flue gas atmosphere. The effect of temperature, humidity and $CO_2$ concentration on the desulfurization of $Ca(OH)_2$ are discussed experimentally. The increasing temperature is not conducive to desulfurization, and the humidity can promote desulfurization, while excessive humidity could inhibit desulfurization. The suitable relative humidity is 20%. In situ generated calcium carbonate has a certain desulfurization effect, but the desulfurization effect is not as good as $Ca(OH)_2$. However, a large proportion of $CaCO_3$ was produced in the desulfurization ash under the condition that $CO_2$ concentration was absolutely dominant to $SO_2$ in the sintering flue gas atmosphere.

**Keywords:** sintering flue gas; semi-dry desulfurization; desulfurization; calcium carbonate; ultra-low emissions



**Citation:** Hong, J.; Zou, X.; Qin, Z.; Zhou, B.; Geng, S.; Zhang, Y.; Zou, X.; Lu, X. Effect of $CO_2$ on the Desulfurization of Sintering Flue Gas with Hydrated Lime. *Materials* **2023**, *16*, 303. https://doi.org/10.3390/ma16010303

Academic Editor: Alain Largeteau

Received: 2 November 2022
Revised: 1 December 2022
Accepted: 23 December 2022
Published: 28 December 2022



## 1. Introduction

The sintering process is a major source of sulfur and nitrogen pollutant emissions of steel mills, and the proportion of $SO_2$ and NOx account for about 60% and 50% of the total emissions from the iron and steel industry, respectively [1,2]. In recent years, the Chinese government strengthened environmental protections, and a series of stricter environmental laws and regulations have been published. With the proposed new concept of "Ultra-low emission", the $SO_2$ and NOx emission standards were changed to <35 mg/Nm$^3$ and <50 mg/Nm$^3$, respectively [3], which were ≤200 mg/Nm$^3$ and ≤300 mg/Nm$^3$ in the 2015 national standard [2].

To match the emission requirements, many methods were applied in iron and steel factories, and the main methods include wet desulfurization technology [4–8], dry desulfurization technology [9,10] and semi-dry desulfurization technology [9]. The semi-dry desulfurization technology has drawn a lot of attention for its advantages of multi-pollutant synergistic control, water saving and low investment in equipment [11]. The mainstream denitrification technologies are SCR (selected catalytic reduction) [12], SNCR (selected non-catalytic reduction) [13], activated carbon adsorption [14] and ozone oxidation–adsorption [11]. Compared with SCR, SNCR and activated carbon methods, the ozone oxidation–absorption method exhibits the advantages of high oxidation selectivity, high oxidation efficiency, and no secondary by-products [15].

Shanghai Meishan Iron and Steel Co. adopted the semi-dry desulfurization technology for simultaneous desulfurization and denitrification from flue gas using a flue gas circulating fluidized bed. Ozone ($O_3$) was introduced to oxidize NO into dioxide ($NO_2$), which is soluble nitrogen and highly active [16]. In the absorption tower, the main component of hydrated lime is $Ca(OH)_2$, the desulfurization rate of sintering flue gas reaches 98% and the denitrification rate reaches 88%, and those meet the requirements of ultra-low emissions for sintering flue gas pollutants.

However, there is a significant increase in the desulfurization ash production under the "ultra-low emission" working conditions, from the original 1349.8/t to 2101.6/t, an increase of about 55.7%. Meanwhile, the composition of $CaCO_3$ in desulfurization ash also increased from 31.17% to 51.50%, an increase of 65.2%, which not only increased the usage of hydrated lime but also imposed a burden on waste disposal and risked potential environmental pollution. Therefore, it is necessary to know the mechanism of $CaCO_3$ increase under a high oxide atmosphere.

Hydrated lime is an adsorbent commonly used in semi-dry desulfurization; $NO_2$ and $SO_2$ react with hydrated lime, curing to form nitrates and sulfates [17–24]. The main components of the sintering flue gas are $SO_2$ 1026~1321 mg/Nm$^3$, NOx 271.4~293.5 mg/Nm$^3$, $O_2$ 15.5~16.5 vol%, $CO_2$ 6.1~7.0, $H_2O$ 10.1~10.9 vol% and dust 28.6~39.0 mg/Nm$^3$. The components of $CO_2$ contribute to the generation of a large amount of $CaCO_3$. For a long time, $CO_2$ has not received attention, and there are few studies on the change in $CaCO_3$ in the desulfurization ash. $CaCO_3$ as an adsorbent is mainly used in the high-temperature stage of 800~1200 °C, which decomposes to CaO to complete the desulfurization reaction [25,26]. For the sintering flue gas temperature conditions (80~120 °C), whether $CaCO_3$ has the effect of desulfurization in the absorption tower has not been clarified.

In this paper, hydrate was selected as the absorbent because it is widely used in the semi-dry desulphurization process in steel works. $CO_2$ contained in the sintering flue gas is a very important factor that needs to be studied. A study focusing on the effect of $CO_2$ in desulfurization was conducted. The competitive reaction of the gas components $SO_2$ and $CO_2$ in sintering flue gas was analyzed thermodynamically. Under the simulated sintering flue gas condition, the effect of $CO_2$ concentration, temperature and relative humidity on the desulfurization of calcium-based adsorbent were carried out. The mechanism of $CaCO_3$ formation and its effect of desulfurization under low temperatures were investigated. The research results will help to understand the mechanism of the formation of desulfurization ash under ultra-low emission conditions.

## 2. Materials and Methods

### *2.1. Experimental Materials*

The raw material used in this paper is quicklime, provided by Meishan Iron and Steel Plant (Nanjing, China). The powdered raw material obtained after grinding and crushing was added to deionized water for digestion, and then the finished suspension was dried to constant weight, and finally the adsorbent was crushed and sieved. As shown in Figure 1a, the original quicklime was mainly composed of CaO, $CaCO_3$ and $Ca(OH)_2$, of which the main ingredient was CaO. The main component of the digested sample was $Ca(OH)_2$ (Figure 1b). The results of laser particle size analysis (Figure 1c) showed that the particle size distribution of original quicklime was 0.5~100 μm, and the average particle size was 7.8 μm, which was consistent with the SEM analysis results (Figure 1d), and the particle sizes were not uniform. The flow chart of making the samples is shown in Figure 1e. A certain amount of samples was taken, and it was ground into powder for XRF element analysis test. The test results are shown in Table 1 It can be seen from the table that raw quicklime contains elements such as Ca, Mg, Fe, Al, Si and K (Table 1). As shown in Table 1, the total calcium content is 88.26 wt.%. The TG-DSC curve of the original quicklime sample is shown in Figure 2, which was obtained in an Ar atmosphere. It is clear that the mass loss process occurs in two different stages. The first stage is at 422.2 °C, which is attributed to the decomposition of $Ca(OH)_2$, while the second stage, at 647.3 °C, shows the decomposition

of $CaCO_3$. According to the mass loss rates $\Delta w_1$ and $\Delta w_2$ of the two temperature segments on the thermogravimetric map, the mass fractions of $Ca(OH)_2$ and $CaCO_3$ can be roughly obtained; the calculation formula of $Ca(OH)_2$ content is $w = \Delta w_1 \times 74/18$, and the formula of $CaCO_3$ content is $w = \Delta w_2 \times 100/44$. Therefore, we found that the $Ca(OH)_2$ content is 75.44 wt.% while the $CaCO_3$ content is 12.43 wt.%. The specific surface area of raw quicklime was 3.3850 $m^2/g$ (Figure 3a), with a relatively uniform pore size distribution and an isothermal adsorption curve close to type IV with an obvious H3-type hysteresis loop.

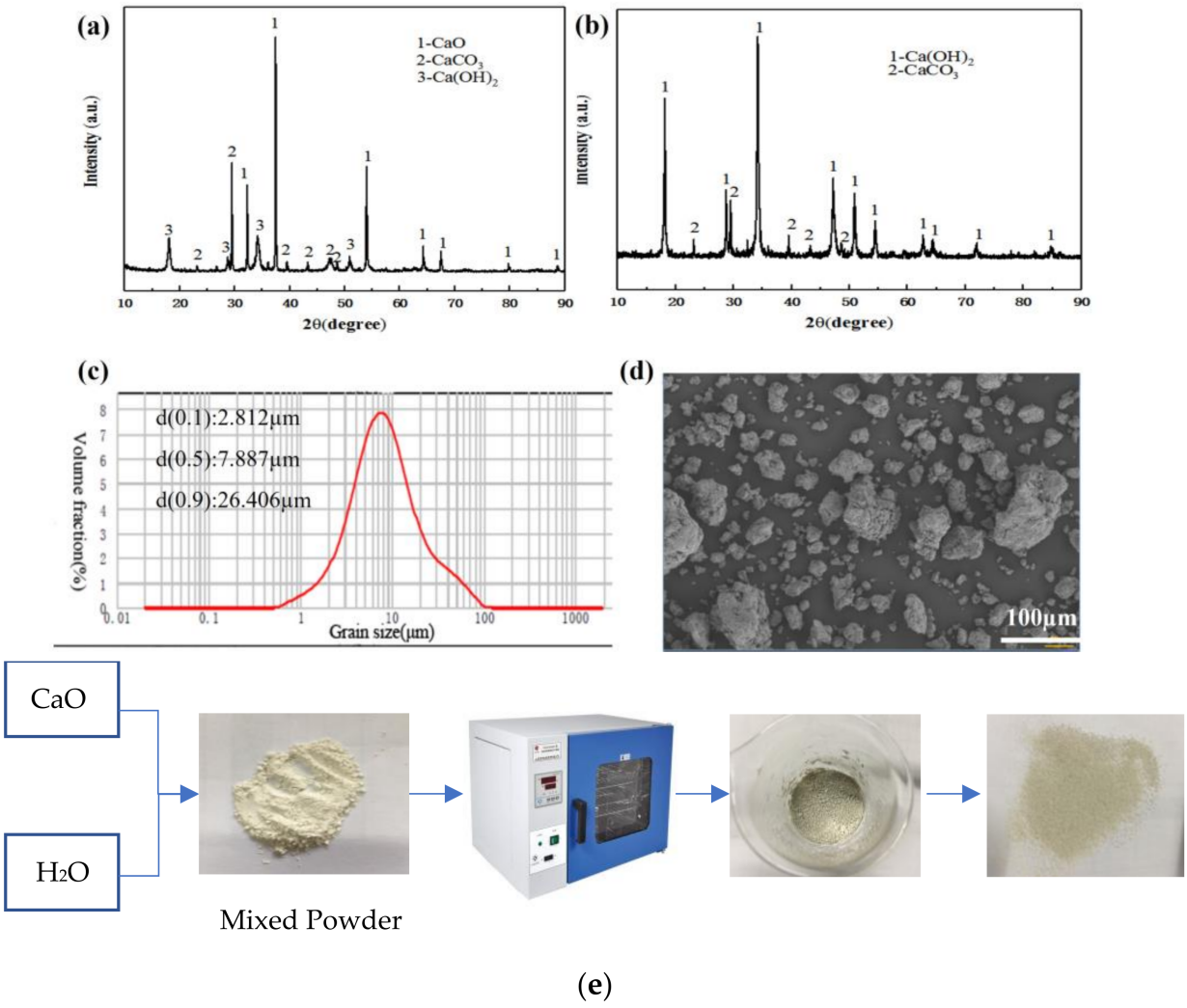


(**e**)

**Figure 1.** (**a**) XRD of raw quicklime; (**b**) XRD of digested sample; (**c**) particle size distribution of quicklime; (**d**) SEM; (**e**) the flow chart of the sample production processes.

**Table 1.** XRF element analysis of dried quicklime samples (wt.%).

| Elements | Ca | Mg | Fe | Al | Si | K |
|---|---|---|---|---|---|---|
| Wt.% | 88.26 | 0.83 | 0.62 | 0.47 | 0.35 | 0.23 |

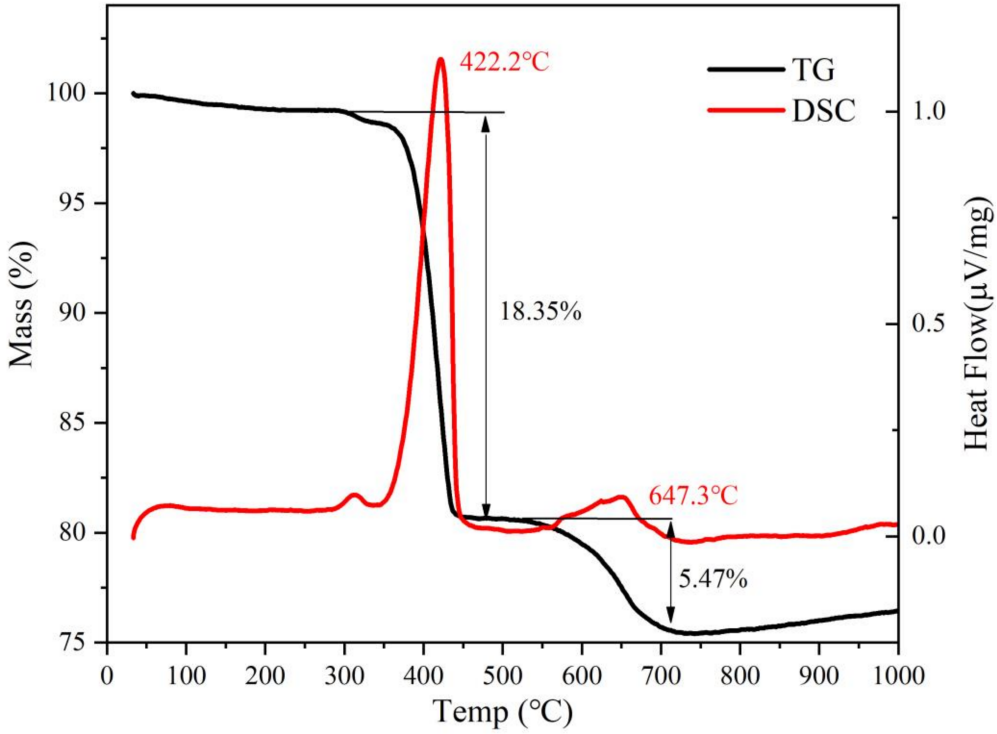


**Figure 2.** TG-DSC curves of raw quicklime.

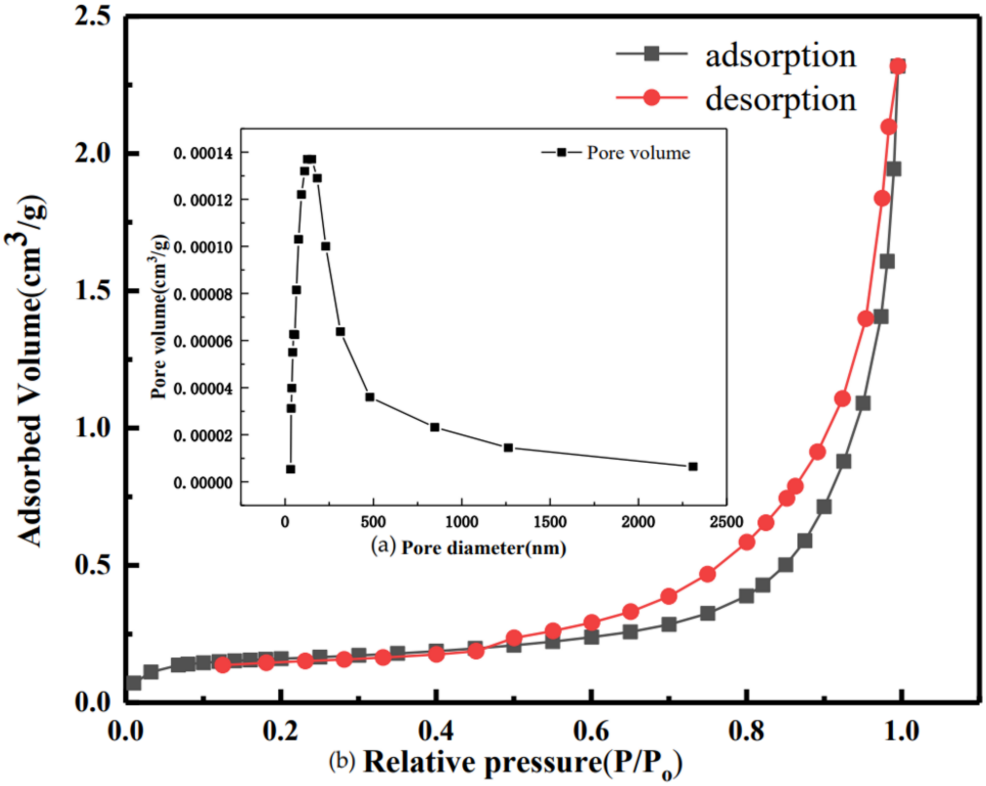


**Figure 3.** Isothermal adsorption and desorption curves (**a**) and pore size distribution curve (**b**) of quicklime.

### *2.2. Experimental Methods*

#### 2.2.1. Experimental Device

The schematic diagram of the experimental system is shown in Figure 4. The high-purity gases ($N_2$, $SO_2$ and $CO_2$) from the high-pressure cylinder are mixed in the mixing tank. The specific purities of gases are listed in Table 2. The composition of the simulated blast furnace gas is controlled by mass flow controller (MFC). The simulated flue gas reacted with the calcium-based adsorbent in the tubular heating furnace. The gas composition was detected by a Testo 350 flue gas analyzer. The gas from the measuring system then passed through the tail gas absorption with the $Na(OH)_2$ solution to remove the acidic components of the tail gas.

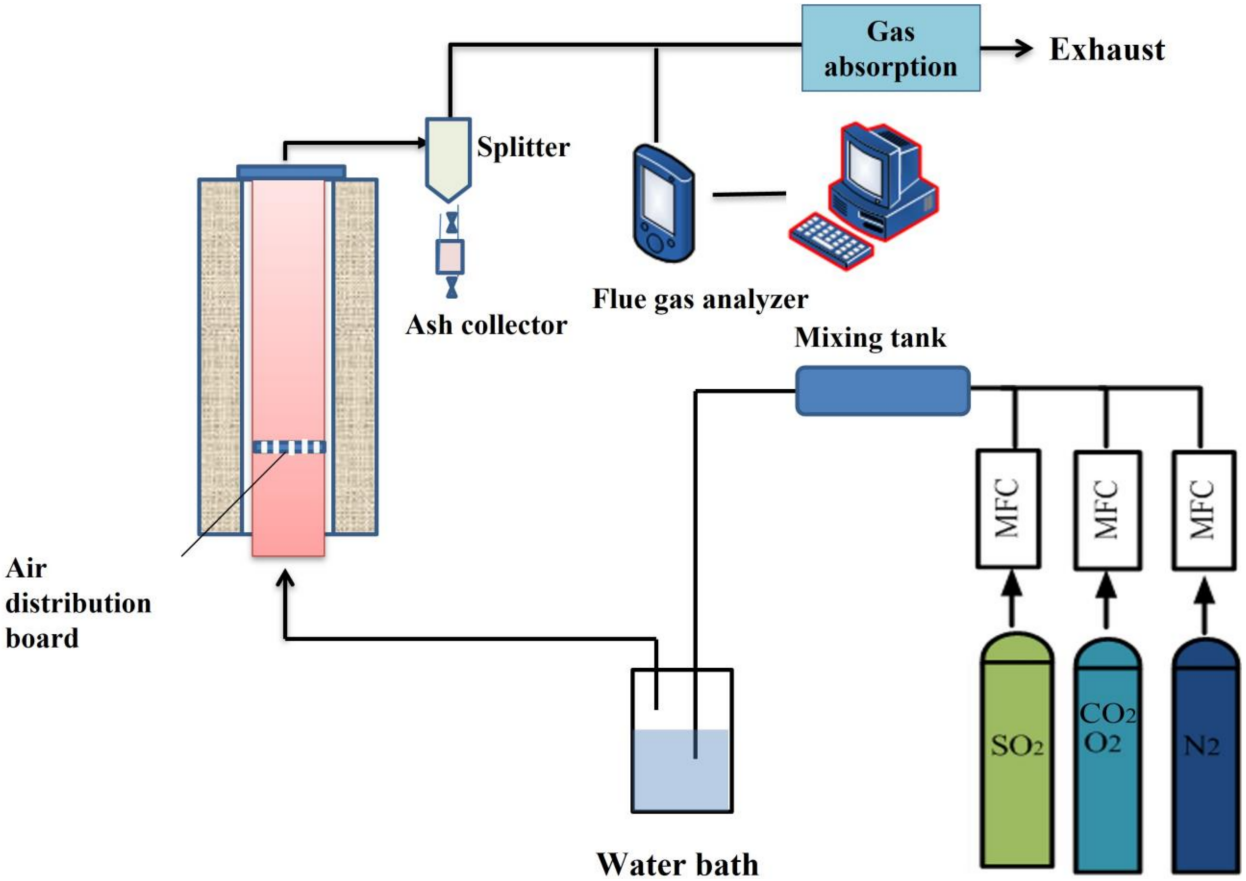


**Figure 4.** Schematic diagram of experimental system.

**Table 2.** Gas composition and flow rate

| Gas Type | Mixed Gas | $SO_2$ | $N_2$ |
|---|---|---|---|
| Concentration | 10%$CO_2$ + 5%$O_2$ + surplus $N_2$ | 4200 ppm | 99.99% |

#### 2.2.2. Experimental Methods

1. Relative humidity calculation

Previous studies have shown that $Ca(OH)_2$ cannot react directly with $SO_2$ in an absolutely dry environment [27,28], so water is introduced into the desulfurization reaction by the water vapor carrying method.

The principle of this method is based on Dalton's law of partial pressure, and the relative humidity is controlled by adjusting the temperature of the constant temperature water bath. The water bath is heated to a set temperature, maintained for a certain time, and the inert gas $N_2$ was introduced into the water through the pipeline and bubbled in

the water to saturate the water vapor, so as to obtain the humidity conditions required for the experiment. The specific calculation of relative humidity is shown in Equation (1).

$$H = \frac{0.622p\delta}{p_0 - p\delta} \tag{1}$$

H—Absolute humidity in grams per kilogram ($g \cdot kg^{-1}$).
P—Saturation vapor pressure of water in Pa (Pa).
Δ—Relative humidity in percent (%).
P0—The total pressure of wet air in Pa (Pa).

2. Desulfurization ash composition analysis

Since there is no corresponding standard for the analysis of desulfurization ash components, the component analysis methods are mainly established based on GB176-1996 "Methods of Analysis of Cement" and GB/T5484 "Methods of Chemical Analysis of Gypsum". The calcium hydroxide content and calcium carbonate content are quantitatively analyzed by thermogravimetry, and the calcium sulfite content is determined by the iodometric method.

2.2.3. Evaluations

The evaluations of the desulfurization effect of adsorbent in the experiments are defined as follows.

1. Desulfurization efficiency

The specific calculation of desulfurization efficiency is shown in Equation (2).

$$\eta_{So_2} = \frac{C_{SO_2,in} - C_{SO_2,out}}{C_{SO_2,in}} \times 100\% \tag{2}$$

$\eta$—The desulfurization efficiency (%).
$C_{SO_2,in}$—The concentration of $SO_2$ in the inlet reactor flue gas, $mg/Nm^3$.
$C_{SO_2,out}$—The concentration of $SO_2$ in the outlet reactor flue gas, $mg/Nm^3$.

2. Penetration time

When the $SO_2$ concentration of tail gas is higher than 35 $mg/Nm^3$, which is the limitation of the national standard, the adsorbent is penetrated and ineffective, and the elapsed time is defined as the adsorbent penetration time.

3. Penetration sulfur capacity

The ratio of the absorbed sulfur mass by penetration to the original adsorbent mass is defined as the theoretical sulfur capacity. The specific calculation of theoretical sulfur capacity is shown in Equation (3).

$$Ps = \frac{Ms}{Mt} \times 100 \tag{3}$$

$P_S$—The penetration sulfur capacity, g/100 g adsorbent.
Ms—The absorbed sulfur mass by penetration, g.
Mt—The original adsorbent mass, g.

2.2.4. Characterization Methods

The particle size distribution (PSD) tests of raw materials were carried out by a laser particle size analyzer (Malvern PANalytical, Mastersizer 2000 MU, The Netherland). The phase composition was characterized by X-ray diffraction (XRD, Bruker-AXS D8 Advance, Billerica, MA, USA) using Cu Kα radiation (λ = 1.54056 Å) at a scan rate of 4° $min^{-1}$ from 10 to 80° (2θ). The microscopic observations and analyses were performed by scanning electron microscope (SEM, FEI Nova Nano SEM 450, Hillsboro, OR, USA). Before being

transferred into the test chamber, the specimens were sputtered with gold coating on the surface. Thermal analysis was conducted using thermogravimetric analysis combined with differential scanning calorimetry (TG-DSC, NETZSCH STA449 F3, Selb, Germany). The purge gas used for TG-DSC was $N_2$, and the heating rate was set to 10 °C/min. The temperature rise range was set at 100~1100 °C.

Gas compositions were analyzed by a Testo 350 flue gas analyzer. The device is widely used in the analysis of plant flue gas for its small size, high sensitivity and portability. Meanwhile, it can measure a variety of complex gas components at the same time without interference. The analyzer adopted electrochemical principles, using the gas at the corresponding oxidation potential for potential electrolysis, and then calculated the concentration of the gas by the current consumed.

## 3. Results and Discussion

### *3.1. Thermodynamic Calculation*

The main components of the sintering flue gas are $N_2$, $CO_2$ and CO, and the main composition of the adsorbent is $Ca(OH)_2$. In the temperature range of the sintering flue gas (80~120 °C), $N_2$ and CO do not react with hydrated lime and are treated as inert gases. The desulfurization reaction of the sintering flue gas is mainly the reaction of $SO_2$ with $Ca(OH)_2$, as shown in reactions (4) and (5). In the flue gas, there is about 6~7 vol% $CO_2$, which can also react with $Ca(OH)_2$ (reaction (6)), forming a competitive relationship with $SO_2$. Figure 5 shows the $\Delta G^{\theta}$-T relationship of these chemical reactions. In addition, the generated $CaCO_3$ has a removal effect on $SO_2$, which occurs in reactions (7) and (8). Thermodynamically, the desulfurization capacity of $Ca(OH)_2$ is higher than that of $CaCO_3$. In the presence of high oxygen potential, it is easier to produce $CaSO_4$, a stable sulfate, which is more favorable for $SO_2$ removal.

$$Ca(OH)_2(s) + SO_2(g) = CaSO_3 + H_2O \quad (4)$$

$$2Ca(OH)_2 + 2SO_2(g) + O_2(g) = 2CaSO_4 + 2H_2O(g) \quad (5)$$

$$2Ca(OH)_2 + 2CO_2(g) = 2CaCO_3 + 2H_2O(g) \quad (6)$$

$$CaCO_3 + SO_2(g) = CaSO_3 + CO_2(g) \quad (7)$$

$$CaCO_3 + SO_2(g) + 1/2O_2(g) = CaSO_4 + CO_2(g) \quad (8)$$

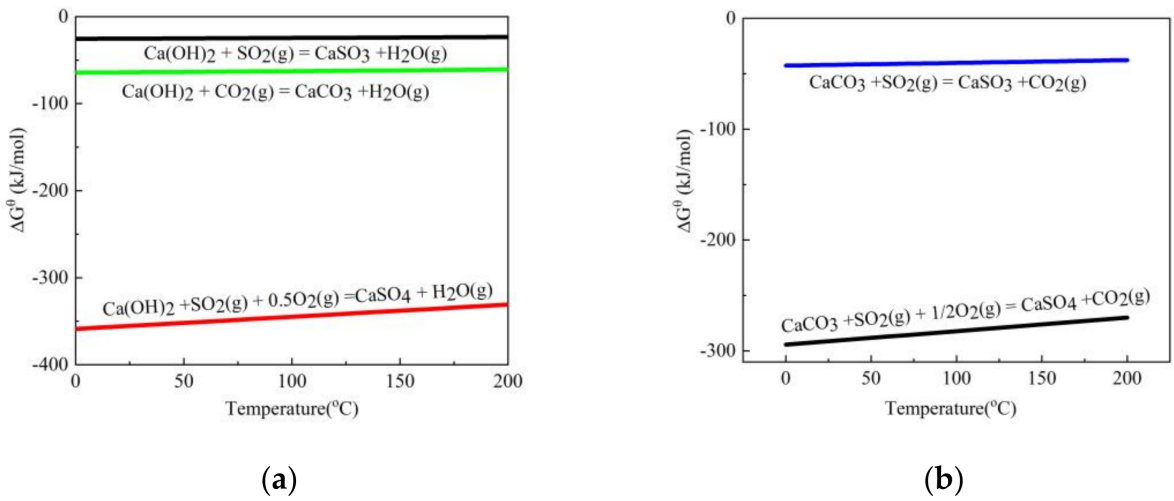


(**a**) (**b**)

**Figure 5.** The $\Delta G^{\theta}$-T diagram of chemical reactions of (**a**) $Ca(OH)_2$ and mixed gas; (**b**) $CaCO_3$ and mixed gas.

### 3.2. Effect of Temperature on Desulfurization Performance of Adsorbent

In the absorption tower, the temperatures of the sintering flue gas at the entrance and exit are about 120 and 80 °C, respectively. To simulate the actual temperature of the absorption tower, the desulfurization temperatures were set as 80 °C, 100 °C and 120 °C, respectively. The carrier gas $N_2$ flow rate was set to 1000 mL/min, the $SO_2$ flow rate was set to 500 mL/min, and the adsorbent loading was 2 g. Figure 6 shows the desulfurization curves of the adsorbent at different temperatures.

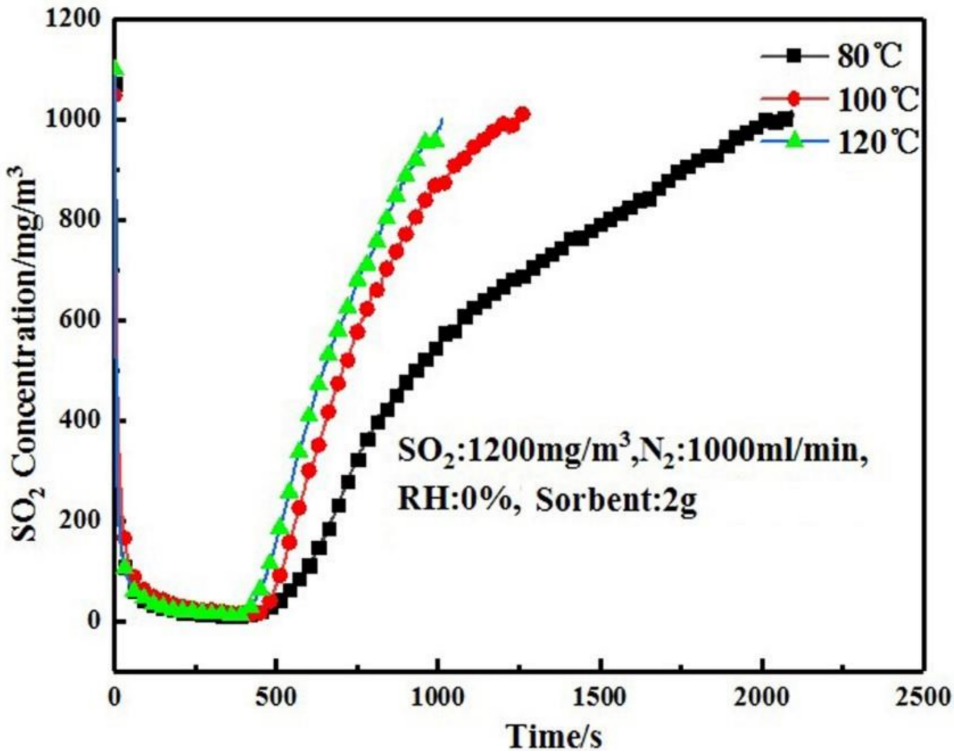


**Figure 6.** Effect of temperature on desulfurization performance of adsorbent (RH = 0%, $SO_2$ = 1200 mg/Nm$^3$).

It can be seen from Figure 6 that the increase in desulfurization temperature was unfavorable for the desulfurization process, and the penetration time became shorter with the increase in temperature. The penetration time was 573 s under 80 °C and 471 s at 120 °C, with a difference of 102 s. As the temperature increased, the desulfurization capacity was decreased, and the utilization rate of the adsorbent decreased. This is due to the fact that the increase in temperature reduces the solubility of $SO_2$ in water, which in turn reduces the concentration of $SO_2$ on the surface of the adsorbent, making the sulfur capacity lower.

### 3.3. Effect of $CO_2$ Concentration on Desulfurization Performance of Adsorbent

The effect of $CO_2$ concentration on the desulfurization penetration time was studied by varying the $CO_2$ content in the gas mixture to 0%, 2.5%, 5.5% and 7.5%, where the reaction temperature was set at 80 °C and the inlet $SO_2$ concentration was kept at 1200 mg/Nm$^3$. The experimental results are shown in Figure 7a. With the increase in $CO_2$ content, the penetration time of the adsorbent decreased significantly. Under the condition without $CO_2$, the penetration time of the adsorbent reached 2500 s. With the addition of 2.5% $CO_2$, it plummeted to 600 s. Further increasing the $CO_2$ concentration, the penetration time did not drop proportional to the $CO_2$ content.

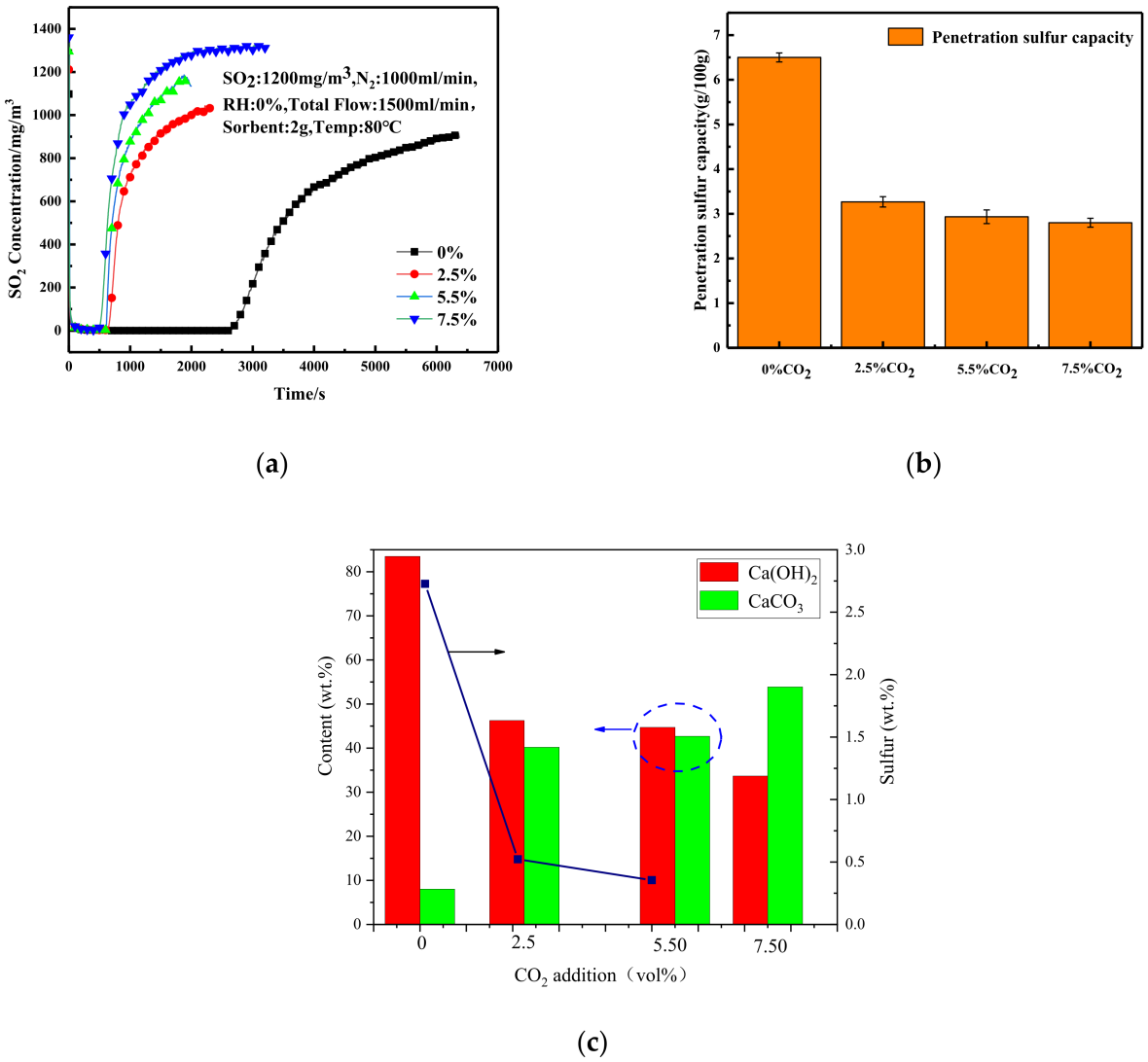


**Figure 7.** Effect of $CO_2$ concentrations on (**a**) desulfurization performance; (**b**) sulfur penetration capacity; (**c**) relative content of $Ca(OH)_2$ and $CaCO_3$ in desulfurization as4. Effect of relative humidity on desulfurization performance of adsorbent

Figure 7b shows the penetration sulfur capacity of desulfurization agents with different $CO_2$ concentrations, and it can be seen that as the $CO_2$ concentration increases, the overall sulfur capacity shows a decreasing tendency. When the $CO_2$ content is 0%, the penetration sulfur capacity reached the maximum value of 6.5 g/100 g adsorbent, which means that the desulfurization effect of the adsorbent is the best at this time. When the $CO_2$ content was increased to 2.5%, it was obvious that the penetration sulfur capacity significantly decreased to only 3.3 g/100 g desulfurization agent, and the penetration time was also shortened, indicating that the $CO_2$ in the gas hinders the desulfurization process of the desulfurization agent and affects the desulfurization performance of it. When the $CO_2$ content was further increased to 7.5%, there was a small decrease in the penetrating sulfur capacity, but not as drastic as before, indicating that $CO_2$ has a decreasing effect on the absorption effect of desulfurization agent, and with the increase in $CO_2$ concentration, there is a plateau, and the decreasing effect is weakened.

With the increase in $CO_2$ concentration, the penetration time of the adsorbent was slightly shortened, the relative content of $Ca(OH)_2$ decreased, and the relative content of $CaCO_3$ increased, as shown in Figure 7c. The S content in the desulfurization ash was decreased, indicating that the desulfurization capacity of the adsorbent decreased.

Figure 8a shows the effect of different relative humidities on the desulfurization process. When relative humidity was increased from 0 to 20%, the penetration time was increased significantly. When the relative humidity was further increased, the penetration time was decreased. Correspondingly, the sulfur capacity at 20% relative humidity was the highest (Figure 8b). It can be concluded that an appropriate humidity is helpful for increasing the desulfurization effect of sorbents, as the desulfurization effect will be weakened by excessive water. The 20% relative humidity is appropriate in this study: the sulfur capacity of the adsorbent reaches 29 g/100 g.

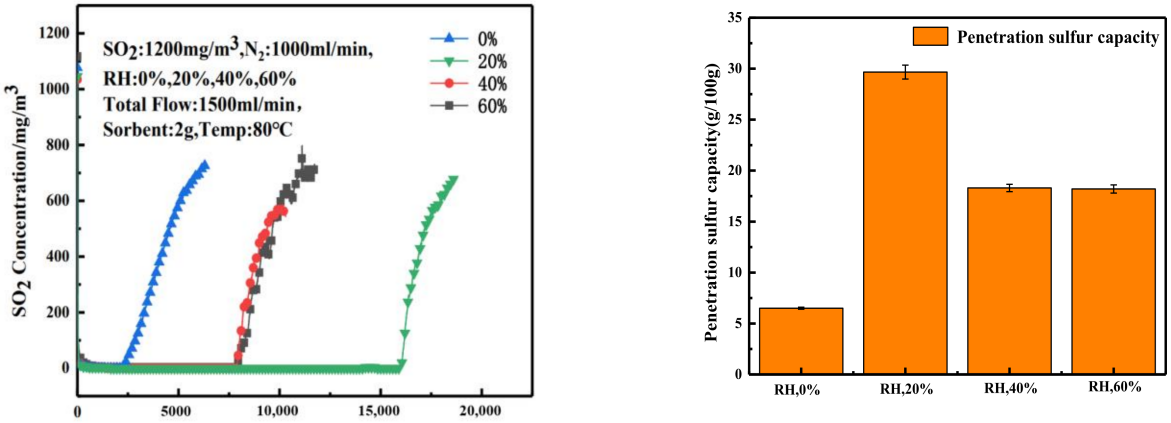


(**a**) (**b**)

**Figure 8.** Effect of relative humidity on (**a**) the desulfurization performance and (**b**) penetration sulfur capacity of desulfurization agent.

### *3.4. Effect of Relative Humidity on Desulfurization Performance of Adsorbent*

#### 3.4.1. Desulfurization Performance of Adsorbent

Under the condition of 20% relative humidity, the penetration time decreased with the increase in $CO_2$ concentration (Figure 9a). The longest penetration time was 1260 s with 2.5% $CO_2$ concentration, and the shortest penetration time was 580 s with 7.5% $CO_2$ concentration. The overall sulfur penetration capacity tends to decrease as the $CO_2$ concentration increases (Figure 9b). This is because the increase in $CO_2$ concentration in the gas mixture consumes the adsorbent, resulting in a decrease in the adsorbent for desulfurization. This indicated that the $CO_2$ concentration weakened the desulfurization effect of the desulfurizing agent at 20% relative humidity, and the sulfur penetration capacity gradually decreased as the $CO_2$ concentration continued to increase.

#### 3.4.2. Morphology and Pore Structure of Desulfurized Ash

As shown in Figure 10a, the surface of the original adsorbent was rough and porous, resulting in a relatively large specific surface area (as shown in Table 3) that was favorable for gas adsorption. After desulfurization in 2.5% $CO_2$ atmosphere (Figure 10b), the pores of the adsorbent became shallow, and there were many crystals growing on the surface. When the $CO_2$ concentration increased to 5.5% (Figure 10c), the surface of the adsorbent obviously became dense and rough. The pores were filled, and the surface was covered with products which had thin strips, flakes, columns, needles and other irregular crystal structures. When the $CO_2$ concentration was up to 7.5% (Figure 10d), the product crystal grew obviously on the adsorbent surface. As a result, the active points of the adsorbent were occupied and the pores were filled by the product, resulting in a decrease in BET and pore volume and pore diameter.

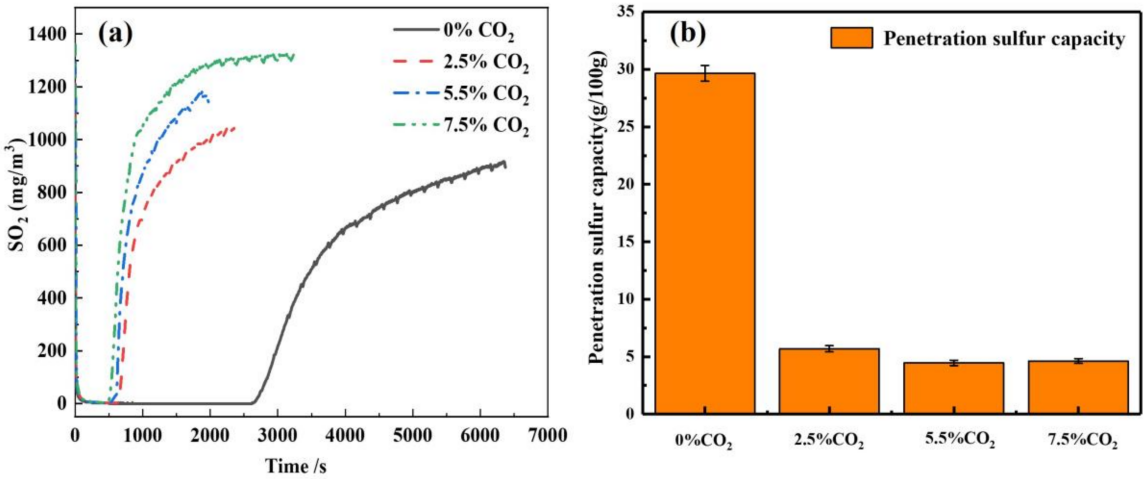


**Figure 9.** (**a**) Effect of different $CO_2$ contents on desulfurization time; (**b**) sulfur penetration capacity of adsorbents at 20% relative humidity.

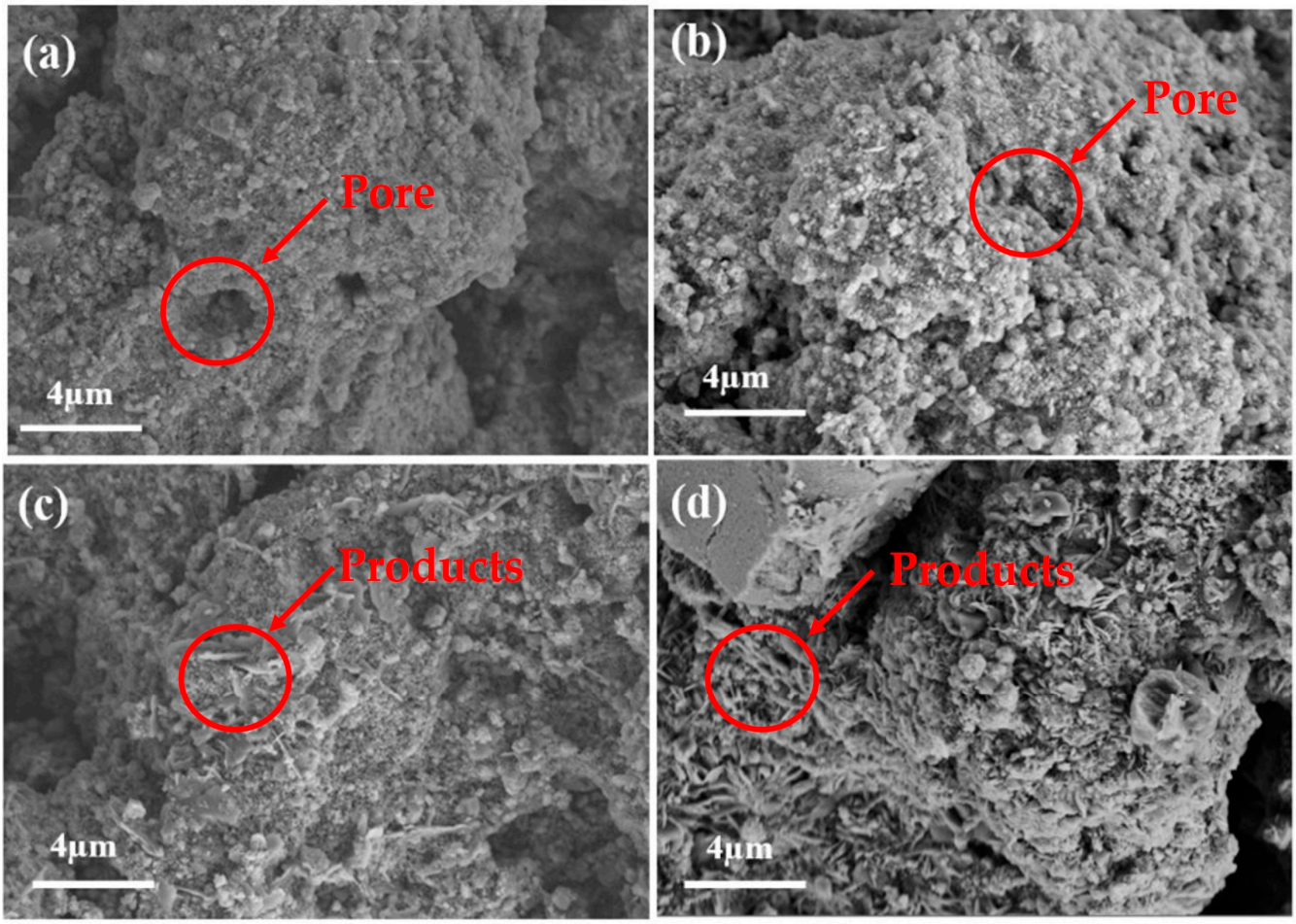


**Figure 10.** Surface morphology of adsorbent: (**a**) original desulfurization; (**b**) 2.5%; (**c**) 5.5%; (**d**) 7.5%.

**Table 3.** BET and pore structure parameters of desulfurization products with different $CO_2$ concentrations.

| Samples | BET Specific Surface Area/$m^2 \cdot g^{-1}$ | Average Pore Size/nm | Pore Volume/$cm^3 \cdot g^{-1}$ |
|---|---|---|---|
| Original adsorbent | 11.74 | 166.14 | 0.049 |
| 0% $CO_2$ | 10.87 | 126.18 | 0.036 |
| 2.5% $CO_2$ | 7.56 | 163.12 | 0.033 |
| 5.5% $CO_2$ | 8.91 | 137.21 | 0.033 |
| 7.5% $CO_2$ | 7.63 | 136.30 | 0.028 |

### 3.4.3. Composition Analysis of Desulfurization Ash

The composition analysis of desulfurization ash is shown in Figure 11a. Without adding $CO_2$, $Ca(OH)_2$ accounted for about 76 wt.% of the desulfurization ash, indicating that the utilization rate of the adsorbent was not high. With the increase in $CO_2$ content in the flue gas, the content of $CaCO_3$ was increased, and the contents of $Ca(OH)_2$ and $CaSO_4$ and $CaSO_3$ were decreased. This is consistent with the results of the TG analysis, as shown in Figure 11b. The weightlessness stages I (330~450 °C) and II (545~750 °C) represented the decomposed $Ca(OH)_2$ and $CaCO_3$. As we can see, with the increase in $CO_2$ content, $Ca(OH)_2$ was decreased and $CaCO_3$ was increased. This is because the concentration of $CO_2$ is much higher than that of $SO_2$. Under the non-equilibrium condition, the formation trend of $CaCO_3$ becomes larger.

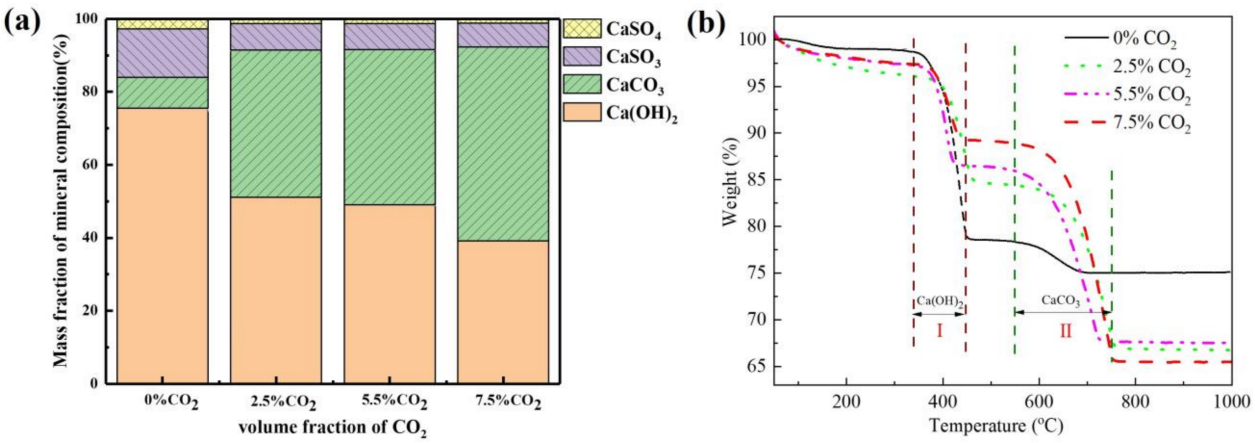


**Figure 11.** (**a**) Composition analysis; (**b**) TG curves of desulfurized ash under different $CO_2$ atmosphere6. The mechanism of $CaCO_3$ on the desulfurization process

From the above analysis, it can be seen that a large amount of $CaCO_3$ was generated with high $CO_2$ concentration in flue gas. To investigate whether in situ generated $CaCO_3$ has a desulfurization effect, a group of experiments was carried out. Firstly, the adsorbent was put in the flue gas containing 5.5% $CO_2$ atmosphere. When the $CO_2$ in the exhaust gas reached stability, it meant the reaction had reached equilibrium, and at this time the surface of the sample was covered with produced $CaCO_3$. Secondly, $SO_2$ was introduced into the flue gas. In order to study the effect of $CO_2$ on desulfurization, two comparative experiments were designed: one for the $CO_2$ + $SO_2$ gas mixture to examine the effect of $CO_2$ on $SO_2$ removal, and the other for cutting off $CO_2$ gas and only passing $SO_2$. The experimental results are shown in Figure 12. The penetration time of in situ generated calcium carbonate as the desulfurization agent under the condition of cutting off $CO_2$ is 405 s, which is higher than that of the $CO_2$ + $SO_2$ gas mixture of 342 s but lower than that of $Ca(OH)_2$ as the adsorbent. It can be seen that the in situ generated $CaCO_3$ has a certain desulfurization ability, but the desulfurization effect is lower than that of $Ca(OH)_2$.

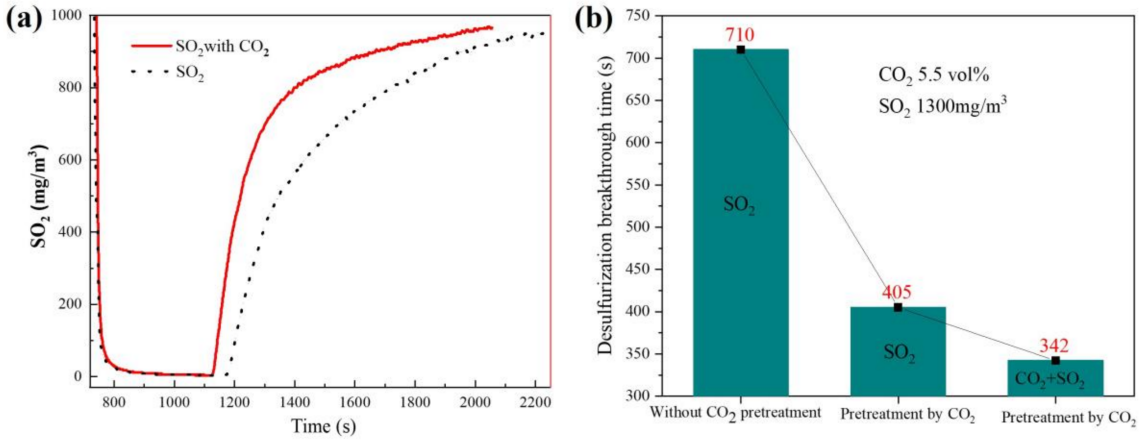


**Figure 12.** Effect of $CaCO_3$ on (**a**) desulfurization and (**b**) desulfurization penetration time under different conditions.

It can be presumed that in the sintering flue gas with high $CO_2$ concentration and strong oxygen potential, $CaCO_3$ and $CaSO_4$ are more easily generated, and the reaction can be divided into three stages as shown in Figure 13. At the first stage, $CO_2$ and $SO_2$ react with $Ca(OH)_2$ at the same time to generate $CaCO_3$ and sulfate, and $Ca(OH)_2$ is continuously consumed as shown Equations (9)–(11). $CaCO_3$ is consumed by reacting with $SO_2$ as in Equation (12), while the generation rate is higher than consumption rate, so the amount of $CaCO_3$ is increasing.

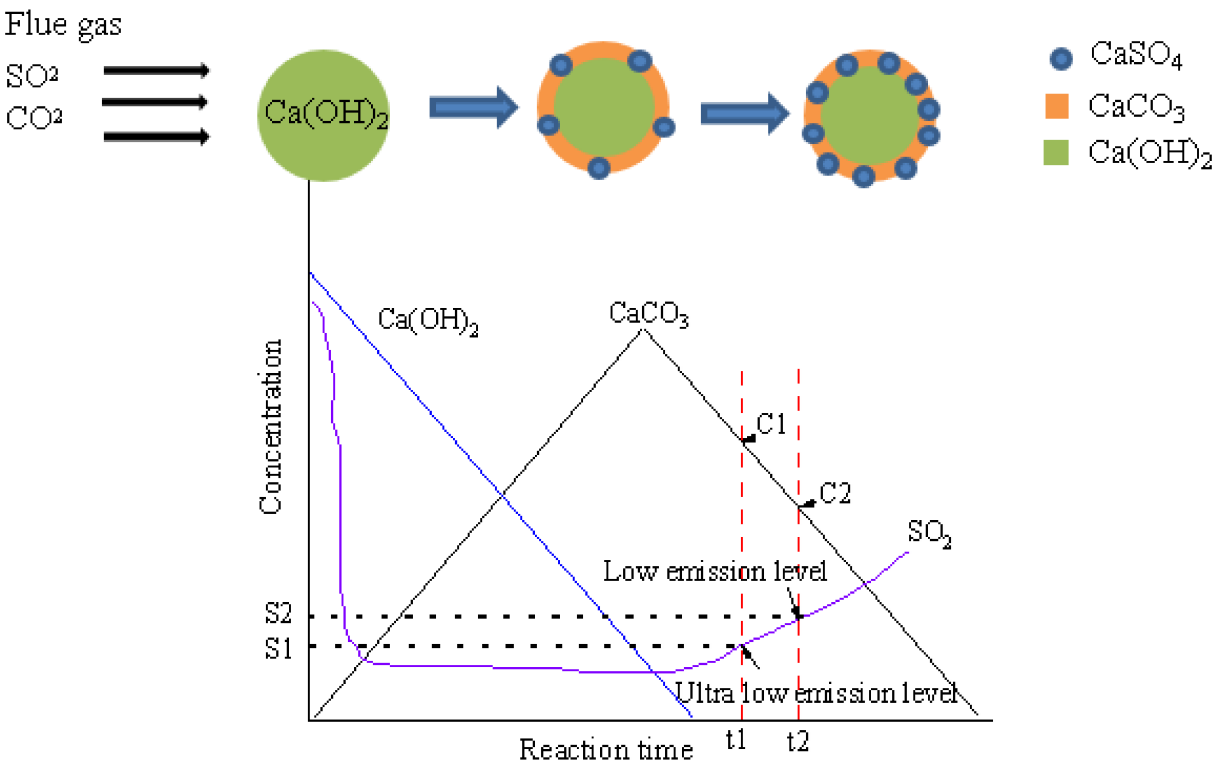


**Figure 13.** Schematic diagram of desulfurization process of sintering flue gas.

At the second stage, $Ca(OH)_2$ is consumed, the surface is wrapped by desulfurization production, and the desulfurization by $Ca(OH)_2$ is weakened. On the contrary, $CaCO_3$ concentration is increased, and $CaCO_3$ is the main desulfurization component as in

Equation (12). After the peak point, the amount of $CaCO_3$ is decreased. At the third stage, the export $SO_2$ concentration exceeds the set value, and the adsorbent fails.

$$CO_2 + Ca(OH)_2 = CaCO_3 + H_2O \quad (9)$$

$$SO_2 + Ca(OH)_2 = CaSO_3 + H_2O \quad (10)$$

$$CaSO_3 + O_2 = CaSO_4 \quad (11)$$

$$SO_2 + CaCO_3 = CaSO_3 + CO_2 \quad (12)$$

After the implementation of the ultra-low emission standard in the steel industry, the limited emitting concentration of $SO_2$ of sintering flue gas was decreased from the original 100 mg/Nm3 to 35 mg/Nm3. As shown in Figure 13, when the emission gas standards are reduced from S2 to S1, the penetration time of the absorbent is decreased from t2 to t1, so more fresh adsorbents are needed, and the corresponding $CaCO_3$ content in the desulfurization ash C1 is also higher than that of C2, which is produced by the original emission standar

## 4. Conclusions

A series of experiments were carried out to study the effect of $CO_2$ on the desulfurization of sintering flue gas with hydrated lime. The main conclusions can be summarized as follows: thermodynamic calculations showed that in the competitive relationship with $Ca(OH)_2$, $SO_2$ reacts more preferentially than $CO_2$ under a thermodynamic standard state, and the desulfurization reaction is easier in the presence of oxygen. The penetration time of the adsorbent decreases with the increase in $CO_2$ concentration, and the decrease is more obvious from the penetration of sulfur capacity, which indicates that $CO_2$ is more likely to generate $CaCO_3$ under the condition of moisture, thus impeding the desulfurization process. In situ generated calcium carbonate may have a desulfurization effect, but the desulfurization effect is not as good as $Ca(OH)_2$.

However, a large proportion of $CaCO_3$ was produced in the desulfurization ash under the condition that the $CO_2$ concentration was absolutely dominant to $SO_2$ in the sintering flue gas atmosphere.

**Author Contributions:** Conceptualization, J.H., Z.Q. and S.G.; methodology, Z.Q., X.Z. (Xinqing Zou), B.Z. and S.G.; formal analysis, J.H. and S.G.; investigation, Z.Q.; resources, J.H. and S.G.; writing—original draft preparation, Z.Q. and X.Z. (Xingli Zou); writing—review and editing, J.H., X.Z. (Xinqing Zou), S.G. and X.Z. (Xingli Zou); supervision, J.H.; project administration, S.G. and Y.Z.; funding acquisition, X.L. All authors have read and agreed to the published version of the manuscript.

**Funding:** This work was supported by the National Natural Science Foundation of China—the joint research fund of China Bao-Wu Iron and Steel Group Co., Ltd. (Grant Nos. U1860108 and U1860203), the National Natural Science Foundation of China (Nos. 52022054 and 51974181), the Shanghai Rising-Star Program (19QA1403600), and the Program for Professor of Special Appointment (Eastern Scholar) at Shanghai Institutions of Higher Learning (TP2019041) for financial support.

**Data Availability Statement:** The data presented in this study are available on request from the corresponding authors. The data are not publicly available due to privacy or ethical restrictions.

**Conflicts of Interest:** The authors declare no conflict of interest.

## References

1. Zhu, T.; Liu, Q.; Li, Y.; Yan, X.; Qi, F.; Ye, M. Emission Characteristics of Multiple Pollutants from Iron- Steel Sintering Flue Gas and Review of Control Technologies. *Sci. Technol. Rev.* **2014**, *32*, 51–56.
2. Ke, X.W.; Cai, R.X.; Lyu, J.F.; Zhang, M.; Wu, Y.; Yang, H.R.; Zhang, H. Research Progress of the Effects of Ca-Based Sorbents on the NO_x Reaction in Circulating Fluidized Bed Boilers. *Clean Coal Technol.* **2019**, *25*, 1–11.
3. Hao, R.; Zhang, Y.; Wang, Z.; Li, Y.; Yuan, B.; Mao, X.; Zhao, Y. An Advanced Wet Method for Simultaneous Removal of $SO_2$ and NO from Coal-Fired Flue Gas by Utilizing a Complex Absorbent. *Chem. Eng. J.* **2017**, *307*, 562–571. [CrossRef]

4. Du, J.; Cao, S. Research Status and Progress of Wet Flue Gas Desulfurization Technology. *Appl. Chem. Ind.* **2019**, *48*, 1495–1500.
5. Ahlbeck, J.; Engman, T.; Fältén, S.; Vihma, M. A Method for Measuring the Reactivity of Absorbents for Wet Flue Gas Desulfurization. *Chem. Eng. Sci.* **1993**, *48*, 3479–3484. [CrossRef]
6. Mohammed, M.Y.; Albayati, T.M.; Ali, A.M. Imidazolium-Based Ionic Liquids for Extraction of Sulfur Compounds from Real Heavy Crude Oil. *Chem. Afr.* **2022**, *5*, 1715–1722. [CrossRef]
7. Mohammed, M.Y.; Ali, A.M.; Albayati, T.M. Choline Chloride-Based Deep Eutectic Solvents for Ultrasonic-Assisted Oxidative Desulfurization of Actual Heavy Crude Oil. *Chem. Eng. Res. Des.* **2022**, *182*, 659–666. [CrossRef]
8. Khadim, A.T.; Albayati, T.M.; Cata Saady, N.M. Removal of Sulfur Compounds from Real Diesel Fuel Employing the Encapsulated Mesoporous Material Adsorbent Co/MCM-41 in a Fixed-Bed Column. *Micropor. Mesopor. Mat.* **2022**, *341*, 112020. [CrossRef]
9. Li, X.; Han, J.; Liu, Y.; Dou, Z.; Zhang, T. Summary of Research Progress on Industrial Flue Gas Desulfurization Technology. *Sep. Purif. Technol.* **2022**, *281*, 119849. [CrossRef]
10. Sun, L.; Li, K.; Tang, L.; Liu, N.; Ning, P.; Sun, X.; Zhang, X. Research Progress of Common Metal Oxides for Flue Gas Desulfurization. *Chem. Ind. Eng. Prog.* **2017**, *36*, 181–188. [CrossRef]
11. Liu, F.; Cai, M.; Liu, X.; Zhu, T.; Zou, Y. $O_3$ Oxidation Combined with Semi-Dry Method for Simultaneous Desulfurization and Denitrification of Sintering/Pelletizing Flue Gas. *J. Environ. Sci.* **2021**, *104*, 253–263. [CrossRef]
12. Wu, Z.; Zeng, Y.; Song, F.; Zhang, S.; Zhong, Q. Active Sites Assembly Effect on $CeO_2$-$WO_3$-$TiO_2$ Catalysts for Selective Catalytic Reduction of NO with $NH_3$. *Mol. Catal.* **2019**, *479*, 110549. [CrossRef]
13. Han, K.; Lu, C. Kinetic Model and Simulation of Promoted Selective Non-Catalytic Reduction by Sodium Carbonate. *Chin. J. Chem. Eng.* **2007**, *15*, 512–519. [CrossRef]
14. Guo, Y.; Li, Y.; Zhu, T.; Ye, M. Effects of Concentration and Adsorption Product on the Adsorption of $SO_2$ and NO on Activated Carbon. *Energy Fuels* **2013**, *27*, 360–366. [CrossRef]
15. Li, B.; Wu, H.; Liu, X.; Zhu, T.; Liu, F.; Zhao, X. Simultaneous Removal of $SO_2$ and NO Using a Novel Method with Red Mud as Absorbent Combined with $O_3$ Oxidation. *J. Hazard. Mater.* **2020**, *392*, 122270. [CrossRef]
16. Ma, Q.; Wang, Z.; Lin, F.; Kuang, M.; Whiddon, R.; He, Y.; Liu, J. Characteristics of $O_3$ Oxidation for Simultaneous Desulfurization and Denitration with Limestone–Gypsum Wet Scrubbing: Application in a Carbon Black Drying Kiln Furnace. *Energy Fuels* **2016**, *30*, 2302–2308. [CrossRef]
17. Liu, C.; Shih, S. A Surface Coverage Model for the Reaction of $Ca(OH)_2$ with $SO_2$ at Low Temperatures. *J. Chin. Inst. Chem. Eng.* **2002**, *33*, 407–413.
18. Lin, R.; Shih, S.; Liu, C. Characteristics and Reactivities of $Ca(OH)_2$/Silica Fume Sorbents for Low-Temperature Flue Gas Desulfurization. *Chem. Eng. Sci.* **2003**, *58*, 3659–3668. [CrossRef]
19. Liu, D.; Kuriyama, A. Influence between Desulfurization and Defluorination Reactions Using $Ca(OH)_2$ in the Simulated Coal-Briquettes. *J. Jpn. Inst. Energy* **2019**, *98*, 44–51. [CrossRef]
20. Lin, R.; Shih, S.; Liu, C. Structural Properties and Reactivities of $Ca(OH)_2$/Fly Ash Sorbents for Flue Gas Desulfurization. *Ind. Eng. Chem. Res.* **2003**, *42*, 1350–1356. [CrossRef]
21. Renedo, M.; Gonzalez, F.; Pesquera, C.; Fernandez, J. Study of Sorbents Prepared from Clays and CaO or $Ca(OH)_2$ for $SO_2$ Removal at Low Temperature. *Ind. Eng. Chem. Res.* **2006**, *45*, 3752–3757. [CrossRef]
22. Wang, W.; Hu, M.; Dong, Y.; Ma, C. Study on the Effect of $CO_2$ on the Consumption of Desulfurizing Agent $Ca(OH)_2$ in Flue Gas Desulfurization. *Ind. Eng. Chem. Res.* **2010**, *49*, 1444–1449. [CrossRef]
23. Zhao, R.; Liu, H.; Ye, S.; Xie, Y.; Chen, Y. Ca-Based Sorbents Modified with Humic Acid for Flue Gas Desulfurization. *Ind. Eng. Chem. Res.* **2006**, *45*, 7120–7125. [CrossRef]
24. Ghosh-Dastidar, A.; Mahuli, S.; Agnihotri, R.; Fan, L.-S. Ultrafast Calcination and Sintering of Ca(OH)2 Powder: Experimental and Modeling. *Chem. Eng. Sci.* **1995**, *50*, 2029–2040. [CrossRef]
25. Wang, Z.; Chen, L.; Yue, S.; Wang, C. Microstructure Evolution of Procedural Products during Limestone Simultaneous Calcination/Sulfation. *CIESC J.* **2018**, *69*, 2149–2157.
26. Anthony, E.J.; Granatstein, D.L. Sulfation Phenomena in Fluidized Bed Combustion Systems. *Prog. Energy Combust. Sci.* **2001**, *27*, 215–236. [CrossRef]
27. Gutiérrez Ortiz, F.J.; Ollero, P. A Realistic Approach to Modeling an In-Duct Desulfurization Process Based on an Experimental Pilot Plant Study. *Chem. Eng. J.* **2008**, *141*, 141–150. [CrossRef]
28. Lyu, J.; Huang, L.; Teng, D.; Fu, H.; Li, T.; Chen, H. Effect of Relative Humidity on Dry Flue Gas Desulfurization by Calcium-Based Desulfurizer. *Chin. J. Environ. Eng.* **2020**, *14*, 1563–1569.